Biochimica et Biophysica Acta 1848 (2015) 848–858

Contents lists available at ScienceDirect

Biochimica et Biophysica Acta

journal homepage: www.elsevier.com/locate/bbamem

Computational insight in the role of fusogenic lipopeptides at the onset of liposome fusion

M. Bulacu [a], G.J.A. Sevink [b,*]

[a] Culgi BV, Galileiweg 8, 2333 BD Leiden, The Netherlands
[b] Leiden Institute of Chemistry, Leiden University, P.O. Box 9502, 2300 RA Leiden, The Netherlands

ARTICLE INFO

Article history:
Received 17 September 2014
Received in revised form 3 December 2014
Accepted 9 December 2014
Available online 18 December 2014

Keywords:
Coarse grained molecular dynamics
MARTINI force field
Lipopeptide
Fusion scenario

ABSTRACT

We performed an extensive computational study to obtain insight in the molecular mechanisms that take place prior to membrane fusion. We focused on membrane-anchored hybrid macromolecules (lipid–polymer–oligopeptide) that mimic biological SNARE proteins in terms of liposome fusion characteristics [H. Robson Marsden et al., 2009]; efficient micro-second simulation was enabled by combining validated MARTINI force fields for the molecular building blocks in coarse-grained molecular dynamics (CGMD). We find that individual peptide domains in the hybrid macromolecules bind and partially integrate parallel to the membrane surface, in agreement with experimental findings. By varying several experimental design parameters, we observe that peptide domains remain in the solvent phase only in two cases: (1) for solitary lipopeptides (low concentration), below a threshold area per lipid in the membrane, and (2) when the lipopeptide concentration is high enough for the peptide domains to self-assemble into tetrameric homo-complexes. The peptide–membrane binding is not affected by solvent-induced peptide unfolding, which we mimicked by relaxing the usual MARTINI helix constraints. Remarkably, in this case, a reverse transition to a helical secondary structure is observed after binding, highlighting the role of the membrane as a template (partitioning–folding coupling). Our findings undermine the current view of the initial stages towards fusion, in which membranes are thought to be kept in close apposition via dimerization of individual complementary peptides in the solvent phase. Although we did not study actual fusion, our simulations show that the formation of homomers, which is suppressed in experimental peptide-pair design and therefore believed to be insignificant for fusion, by peptides anchored to the same membrane does play a key role in this locking mechanism and potentially also in membrane destabilization that precede fusion.

1. Introduction

It is generally accepted that a specialized set of proteins plays a key role in overcoming energetic barriers that have been identified for lipid membrane fusion [1]. Understanding membrane fusion thus implies obtaining detailed molecular information on the role of the 'actors' in fusion, in particular on the membrane–protein interaction, protein/protein association, membrane destabilization and merging aspects of the fusion mechanism. One way to reduce the complexity of this task is to introduce a simplified model system that contains only necessary ingredients for biomimetic fusion. Recently Kros [6,7] introduced such a model system with desired fusion characteristics, both lipid and content mixing [7], that holds a promise for targeted drug delivery. This model system consists of liposomes that are decorated with fusogenic lipopeptides LPE or LPK, containing short peptide domains E: $(EIAALEK)_3$ and K: $(KIAALKE)_3$ that induce fusion via an unresolved mechanism that involves peptide self-assembly into E/K coiled-coils. Even for such a simplified fusion model, fundamental understanding is hampered by several unknowns: the protein secondary and quaternary transformations during self-assembly and membrane fusion, the protein interaction with the bilayer and the role of the solvent (e.g. Ca^{2+} ions) in fusion. One key issue in most experimental characterization techniques is that, by probing properties of ensembles of molecules, details at the molecular level remain elusive. X-ray crystallography faces the solubility problem of membrane-associating proteins and other imaging techniques lack appropriate resolution (e.g. NMR). As a result, the atomistic structures of both the membrane and protein complex, before and after assembly as well as during fusion, are difficult to determine.

Since molecular simulation methodology has in recent years matured into a reliable and increasingly efficient tool for studying molecular mechanisms, we believe that computational study can complement the experimental investigations by shedding light into the molecular mechanisms that trigger fusion. We therefore performed a detailed computational study of fusogenic lipopeptides LPE and LPK prior to fusion, concentrating on the overall lipopeptide binding behavior. We use the computational flexibility to assess several anticipated key factors independently, investigating their function in the general locking and

* Corresponding author.
E-mail address: a.sevink@chem.leidenuniv.nl (G.J.A. Sevink).

http://dx.doi.org/10.1016/j.bbamem.2014.12.010
0005-2736/

membrane destabilization mechanisms. Our starting point is the lipopeptide anchored to a membrane, with a lipid/cholesterol composition that matches the experimental conditions [7].

Averaging over molecular degrees of freedom is unavoidable if one wants to realistically capture slow phenomena on a supramolecular scale. The size of the relevant molecular system, combined with the long (μs) simulation time, dictates the use of a coarse-grained (CG) simulation methodology. In the spirit of an earlier lipopeptide study [13], we employed validated coarse-grained MARTINI force fields for lipids [10], proteins [11] and polymers [12,24] and combined them into a unified force field for the hybrid lipopeptide. The coarse-grained MARTINI [10] force-field has been successfully used for simulating a variety of systems, including the longer-term dynamics of an antimicrobial lipopeptide [13] and other transmembrane proteins [15,16] and, very recently, membrane associating proteins [17,18] near a lipid membrane. Moreover, MARTINI is known to accurately reproduce the structural and collective properties of a variety of lipids in the lamellar state [23]. We applied the standard MARTINI constraints to restrain the secondary structure of the two CG peptide domains to the resolved α-helix for the E/K dimer (by NMR), but also considered the effect of relaxing these constraints. Moreover, via simulations that exceed 500 μs total simulation time (see SI for a table), we have studied the significance of experimental factors such as the lipopeptide concentration, the average area per lipid in the membrane and the length of the polymeric spacer between the lipid and the peptide. Whenever possible, results have been compared to detailed measurements. Because of the good agreement between experiments and simulations, we conclude that this CGMD study provides the first detailed insight in the molecular factors that underlie the initial stages of membrane fusion.

2. Methods

All simulations were carried out with the MARTINI coarse-grained model [10–12] using the Gromacs MD package (version 4.5.3) [22], with the usual MARTINI coarse-grained molecular dynamics conditions: time step t = 20 fs, semi-isotropic pressure coupling P = 1 atm and Berendsen thermostat T = 293 K.

The lipopeptide [6–25] is a hybrid macromolecule that links a DOPE lipid with a peptide (E or K) at the C terminus, via a linker formed by one succinic anhydride and a PEG polymer, which can be of varying length. We select a length of 12 monomers, in agreement with the standard experimental setup, but consider other values in the Supporting Information (SI). Our MARTINI representation of the $LP_{12}K$ lipo-peptide is shown in Fig. 1. It combines existing representations of the separate domains — lipid [10], protein [11] and polymer [12] into a unified MARTINI hybrid force-field (see SI for more details). The α-helicity of the peptide domains is imposed through dihedral potentials, with the usual force constant $k = 400$ kJ mol^{-1}, along the backbone beads. The linkers between the domains were treated as covalent bonds with controlled rigidity. Our approach is equivalent to the one applied previously for PEGylated lipids [12] and a shorter lipopeptide [13], but it is for the first time that a three-component (lipid–polymer–peptide) hybrid is simulated.

The membrane consists of 192 DOPC and 96 DOPE lipids, and 96 cholesterol molecules, with relative fractions (2:1:1) chosen to agree with experimental conditions [25]. It was created from an equilibrated pure DOPC membrane [26], by changing a pre-defined fraction of DOPC into DOPE and cholesterol, keeping an equal distribution in the two leaflets. Technically, for DOPE, we changed the NC_3 into the NH_3 bead type and replaced the double bond from each lipid tail by a single bond. Cholesterol is generated by selecting only eight beads from a DOPC lipid and re-assigning their bead types, bonds and angles specific to cholesterol (see Fig. S1 in the SI). Consequently, the membrane is solvated by 10,000 coarse-grained water molecules, with 725 sodium cations and 725 chloride anions (see SI for more information on the salt representation). The setup contains approximately 16,500 coarse-grained particles. The membrane is equilibrated for 5 μs until the structural properties (area per lipid and bilayer thickness) assume constant values. The final area of the simulation box parallel with the standard membrane is 10 nm × 10 nm.

After membrane equilibration, a lipopeptide is incorporated into the membrane-water system, by replacing one of the membrane DOPE lipids with the DOPE domain in the lipopeptide, followed by a removal of overlapping water or ion molecules. A short run is performed, with the lipopeptide fixed, to allow for solvent rearrangement. Subsequently the run is continued with all constraints released and this part of the trajectory is used for analysis. An example of the whole system in the simulation box is shown in Fig. 2.

The sensitivity to initial lipopeptide conformations was considered by simulating ten different instances for each lipopeptide, unless mentioned otherwise; convergence to the same final state was identified in all cases. The starting structures for each peptide were generated by taking ten instances of the NMR solution structure of the heterodimeric coiled-coil complex E–K, PDB ID: 1U0I [27]. The lipopeptide is always initially anchored perpendicular to the membrane, with the polymer linker in an extended conformation.

Atomistic molecular dynamics studies have thus far focused on static and/or short-term dynamical properties, such as the role of stabilizing interactions, and the effect of local amino-acid replacement or environmental factors on oligomerization (see [9] for a recent concise overview) based on the NMR-resolved dimeric E/K structure. In addition to the coarse-grained MD studies, we performed atomistic MD (see SI for simulation details and results) to investigate the secondary structure transition for individual peptides (E and K) in solvent. Since the determination of this atomistic equilibrium peptide conformation is not our target, we focused on the onset of this transition and limited ourselves to 150 ns trajectories.

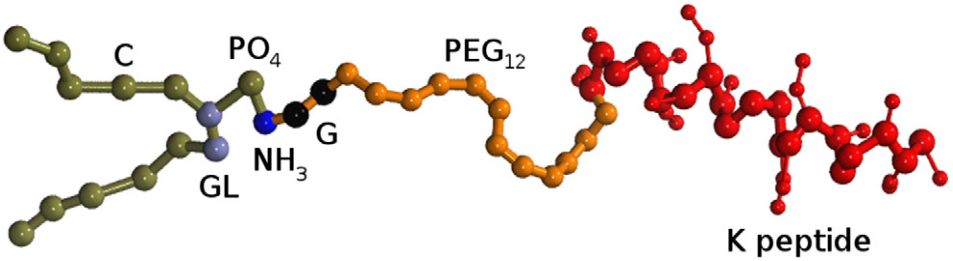

Fig. 1. The coarse-grained model of the lipo-peptide $LP_{12}K$. The lipid is depicted with tan tails and blue/tan/ice blue colored beads for the choline/phosphate/glycerol moieties. The PEG beads are orange and the succinic anhydride is black. The K peptide is represented with red beads, where the size indicates backbone (big) or side chain (small) particles. In the remainder, we use a blue bead representation for the E peptide.

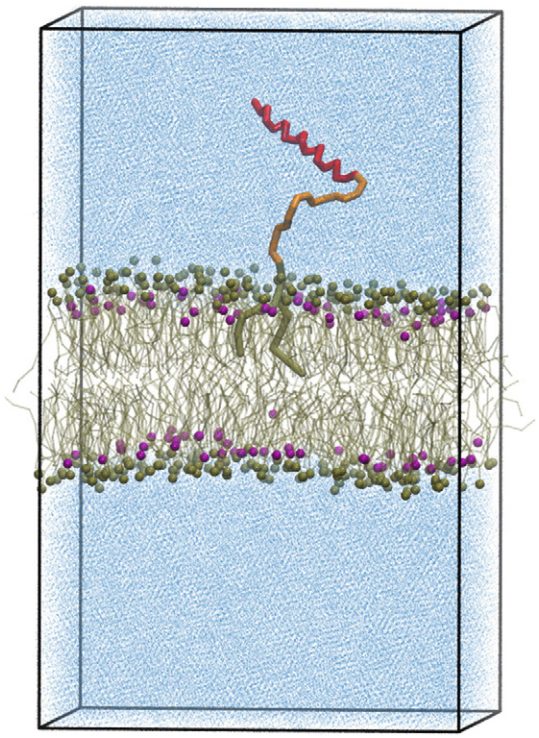

Fig. 2. An example of the simulation box consisting of membrane, $LP_{12}K$ lipo-peptide and solvent. Colors in the $LP_{12}K$ model are used to distinguish between: the peptide (red backbone), the polymer spacer (orange) and the DOPC lipid anchor (tan). In the membrane only the phosphate and the cholesterol ROH beads are displayed in tan and purple. Water and ion particles are shown as a blue haze.

3. Results

3.1. Lipopeptide binding and subsequent effects on membrane properties

Simulations are started from systems prepared as described above, with the peptide domains well outside the membrane, in the solvent phase (see Fig. 2). During the runs, both E and K peptides approach the membrane and completely adhere to its surface in relatively short time. After this, they 'float' on the top of the membrane and the orientation of the α-helix is parallel to the membrane plane, as illustrated in Fig. 3. Owing to the relatively hydrophilic nature of PEG, the spacer is almost completely outside of the membrane. No disattachment was observed in the additional 2.2 μs following peptide insertion. This positioning, somehow expected due to the amphipathic character of the peptide, has been reported in previous atomistic simulations of very similar fusion peptides (influenza hemagglutinin) [29] and determined by InfraRed Reflection Absorption Spectroscopy (IRRAS) measurements for $LP_{12}K$ and LP_{12} E in mono-layers with an identical lipid/cholesterol composition [30].

The timescale at which the peptide adheres to the membrane and positions itself in the final conformation on the membrane is, with a maximum of 0.6 μs, very short compared to the timescale of a fusion experiment. This can be seen from the evolution of the distance, Fig. 4, and the angle, Fig. 5, between the peptide and the membrane. A lipopeptide that is adhered to the center of the PO_4 region, in an orientation parallel to the membrane surface, is characterized by a vanishing distance and angle (see SI for details of the analysis). To illustrate the randomness of the initial lipopeptide conformations, we have added particular values for four out of ten simulations (colored lines) that we performed for each lipopeptide. It is worth stressing that the individual time series also demonstrate that the peptides settle down on the membrane for all initial configurations.

Close visual inspection of the trajectory shows that peptide domains repel the lipid heads beneath it upon approach, and that they insert themselves longitudinally into the lipid headgroup region, between the PO_4 groups. Neighboring lipids have to rearrange their tails to fill the space under the peptide, and do so by bending. Since the fraction of membrane lipids/cholesterol involved in this short-lived stage is almost negligible, quantification on the level of the membrane, for instance via an order parameter, will not produce any notable effect. On a larger scale, however, the membrane undulations become notably enhanced during and after peptide binding.

Averaging over time reveals how peptide binding perturbs the membrane: from 101.64 ± 0.29 nm^2 (total area) and 4.60 ± 0.04 (thickness) for the pure membrane to 102.02 ± 0.43 nm^2 and 4.60 ± 0.07 (with $LP_{12}K$) and 102.04 ± 0.38 nm^2 and 4.60 ± 0.06 (with $LP_{12}E$). Clearly, the effect of binding of single peptides to this membrane patch is small, but since the total content (lipids/cholesterol) of the pure membrane is conserved upon addition of the lipopeptide, the total membrane area is a sensitive measure for peptide incorporation.

Fig. 6 shows time-averaged density or distribution profiles for the I (Ile) and L (Leu) residues (peptides) and for PO_4 and NH_3–NC_3 lipid groups (membrane), for both $LP_{12}K$ and $LP_{12}E$. The profiles for the

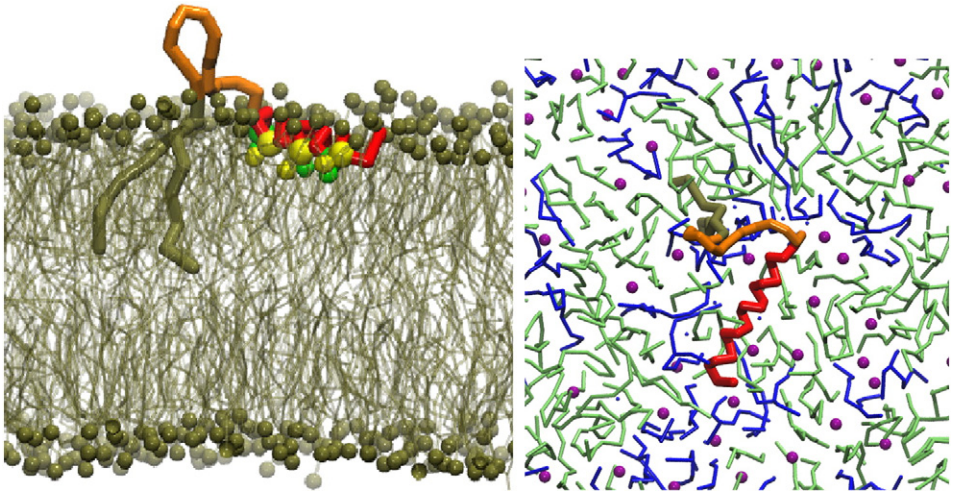

Fig. 3. Lateral view (left) and top view (right) of the final stage of simulation, where the $LP_{12}K$ lipopeptide adheres to the DOPC/DOPE/CH membrane. Colors in the $LP_{12}K$ are used to distinguish between: the peptide (red backbone with green and yellow beads for the Ile and Leu amino acids), the spacer (orange) and the DOPC lipid anchor (tan). In the side view, only the phosphates and lipid tails are shown (in tan). In the top view, the DOPE and DOPC lipids are colored in blue and green, while the head-groups of cholesterol are represented as purple beads.

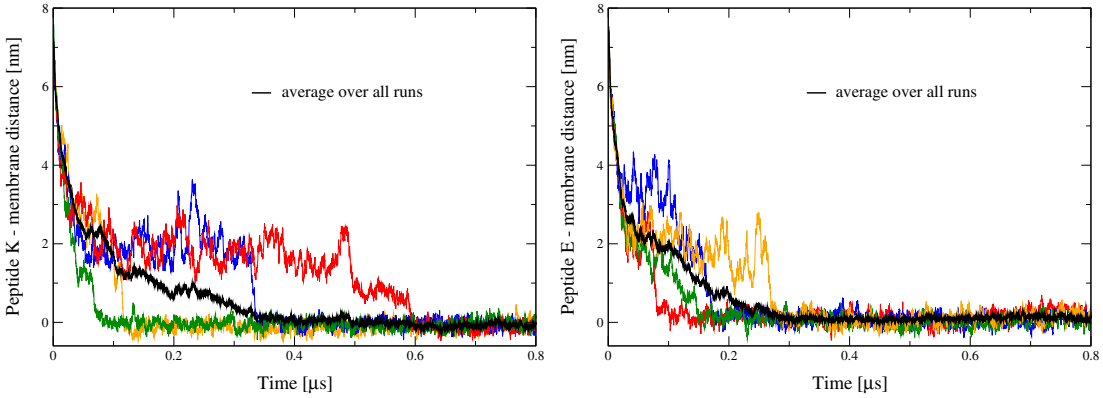

Fig. 4. Evolution of the distance between the center of the mass of the peptide (left, K and right, E) and the center of the mass of the phosphates in the leaflet to which the lipo-peptide is attached. Different colors are used to discriminate between four of the ten independent runs. The average distance is represented in black.

lipid groups are very similar for both cases, corroborating the earlier finding that the perturbation of membrane properties (thickness and area) as a result of E or K peptide attachment is very similar, and we have therefore plotted only one profile for these groups.

It can be seen that peptide K positions itself deeper into the membrane than peptide E (compare the red and blue lines in Fig. 6). This difference is small compared to the characteristic length scales in CGMD, however, in the order of only a few angstrom, and relates to the net positive charge of K and the negative charge of the PO_4 particles. Owing to their hydrophobic character, the Ile and Leu amino-acids in the peptides are most deeply submerged in the membrane (see also Fig. 3, left, green and yellow beads).

3.1.1. Lipid clustering

To investigate the possibility of peptide-induced clustering of membrane constituents around the immersed peptide, we have calculated the radial distribution functions (RDFs) for cholesterol molecules, NC_3, NH_3 and $NH_3 + NC_3$ lipid groups from the leaflet in which the peptide is incorporated. We found it more illustrative if we, unlike standard RDFs, only consider the number of particles in the shell $[r, r + \delta r]$. Disregarding the volumetric scaling gives rise to a function that will not approach unity for large r, but it is equivalent to the actual RDF (by the known scaling) and we disregard this distinction. Moreover, in all cases, distances were determined with respect to the surface of the peptide, i.e. the closest residue in the peptide, and only the component in the membrane plane is considered. By selecting the surface (2D) radial distribution functions, the different peptide indentation depths will not affect the RDFs.

The RDFs for $LP_{12}K$ and for $LP_{12}E$, calculated using snapshots immediately after the peptide adhering and at the end of the extended simulation, are gathered in Fig. 7. It is clear that peptide–membrane interactions affect the structure of the membrane. Moreover, lipids and cholesterols rearrange, supported by undulations, and this rearrangement is found to depend on the peptide nature. We observe enrichment of DOPE around peptide K (compare the red and the orange curves in Fig. 7c), and DOPC enrichment for peptide E (blue and cyan curves in Fig. 7d) with time. Nevertheless, comparing Fig. 7a–b, the overall lipid and cholesterol structure is not much affected by the process of peptide insertion.

3.1.2. Lipid diffusion

Next, we investigated the lateral diffusion along the membrane plane for the lipopeptide and for the lipids in both membrane leaflets, where 'top' stands for the leaflet in which the lipopeptide is incorporated and 'bottom' for the opposite leaflet without the lipopeptide. The lateral diffusion constant D (see Table 1) was determined from the limiting behavior of the measured mean-square displacement, using the Einstein relation for two-dimensional (lateral) diffusion.

The first observation is that our coefficients for lateral self-diffusion in pure membranes agree well with earlier determined values for different lipids and cholesterol mixtures, calculated using the same MARTINI model [31]. In the pure membranes, however, we identify a considerable spread for the lipid diffusion coefficients between two identical leaflets, which quantifies the precision of this analysis and may suggest that there is no significant effect of lipopeptide attachment. Nevertheless, we note again that the fraction of peptide-surrounding lipids is small in all cases. The lipid diffusion in the 'top' leaflet can be seen to be retarded for DOPE lipids (for $LP_{12}K$) and DOPC lipids (for $LP_{12}E$), which agrees very well with the peptide-specific lipid clustering that was found from the RDFs. It suggest that lipids in these clusters move

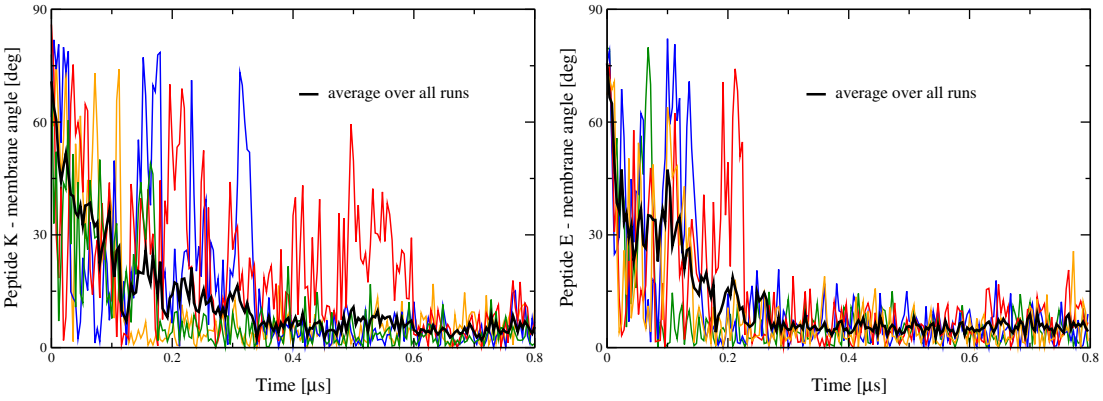

Fig. 5. Evolution of the angle between the principal axis of the peptide (left, K and right, E) and the membrane interface. The averaging procedure (10 simulations) and color scheme are the same as in Fig. 4.

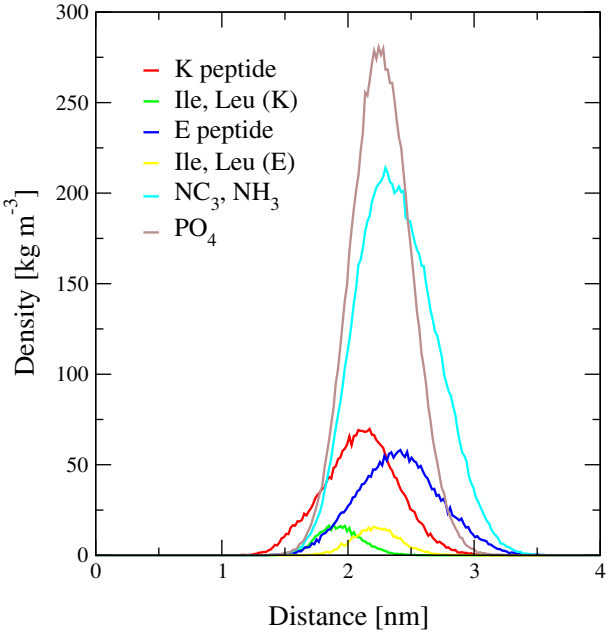

Fig. 6. Particle density profiles for: the K peptide (red) and its Ile and Leu residues (green); the E peptide (blue) and its Ile and Leu residues (yellow); lipid residues PO_4 (brown) and NH_3–NC_3 (turquoise). For the latter, we only considered the leaflet where the peptide is incorporated. Distances were calculated with respect to the dividing plane between the two leaflets (= the origin). The densities are the result of averaging over the end of the extended trajectory, during which both peptide domains adhere well to the membrane.

in concert with the peptide, diffusing at a much lower rate than 'free' lipids. Although the mean-square displacement curves for the peptides do not really become linear within simulation time, the estimated lateral diffusion coefficients are also listed and are indeed quite small (roughly a factor of four–five) compared to 'free' lipids.

In conclusion, we find that both lipopeptides bind to the membrane, with the K peptide domain adhering deeper into the membrane than the E peptide domain. This finding agrees with the amphipathic character of K, predicted by the classification of Segrest [38,39] based on the charge distribution in the α-helical state. We note that the distribution of (negative) charges in E falls outside this classification system. The binding depth signals a higher membrane affinity for K than for E, in full agreement with experiments. The perturbation of the membrane properties due to peptide binding is rather modest for both

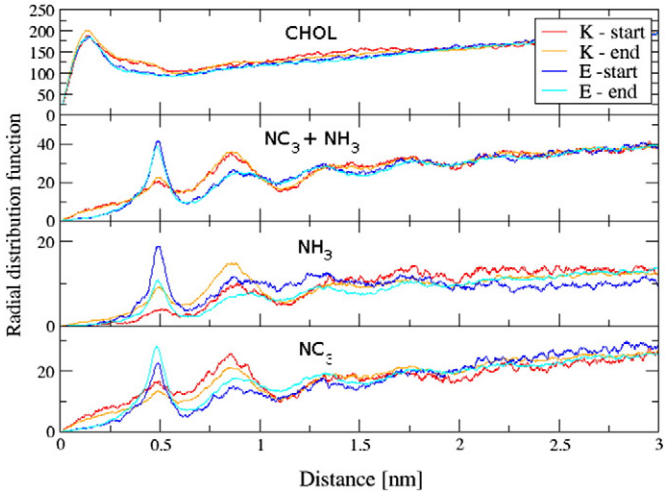

Fig. 7. Lateral radial distribution function between the peptide surface and (a) cholesterol, (b) $NH_3 + NC_3$, (c) NH_3 and (d) NC_3, at the beginning and the end of the simulation with the peptide onto the membrane.

Table 1
Lateral diffusion coefficient D [10^{-7} cm^2/s] along the membrane plane for DOPC and DOPE lipids, and for the lipopeptides. Lipid diffusion coefficients have been differentiated with respect to the leaflet: up — in the leaflet to which the peptide is anchored, down — pure leaflet (T = 293 K).

	DOPC		
	Total	Top	Bottom
Membrane	1.48 ± 0.14	1.32 ± 0.25	1.64 ± 0.03
With $LP_{12}K$	1.42 ± 0.11	1.40 ± 0.02	1.45 ± 0.23
With $LP_{12}E$	1.44 ± 0.06	1.24 ± 0.24	1.64 ± 0.13
	DOPE		
	Total	Top	Bottom
Membrane	1.50 ± 0.39	1.57 ± 0.61	1.44 ± 0.18
With $LP_{12}K$	1.51 ± 0.15	1.18 ± 0.22	1.84 ± 0.08
With $LP_{12}E$	1.66 ± 0.19	1.52 ± 0.31	1.80 ± 0.08
	Lipopeptide		
Membrane	—		
With $LP_{12}K$	0.32 ± 0.10		
With $LP_{12}E$	0.29 ± 0.42		

lipopeptides, which can be expected for a localized effect for a solitary lipopeptide. While membrane fluctuations are enhanced on a larger scale, we identified a localized peptide-dependent lipid structuring around the peptide. We found evidence for a concerted movement of such a cluster, giving rise to diffusion that is significantly slower than the diffusion of lipids in other parts of the membrane.

3.2. Increasing the lipopeptide concentrations: the role of homomers

Destabilization of homomers, e.g. E/E and K/K, via carefully selected electrostatic interactions, was an important design criterion for the E and K peptide pair. This criterion is based on the concept that homomers do not play a role in fusion, meaning that their formation should be avoided. Nevertheless, there is ample experimental evidence that such aggregates do form [25–30]. The considered solitary lipopeptides thus represent a limiting case, quantified by the number of anchors $n_a = 1$, and it is relevant to consider the situation $n_a > 1$, i.e. systems where peptide–peptide interactions play a role. The formation of a complex by two or more of the same peptide domains, either in solution or in the membrane, will shield the hydrophobic domains that are present in each of the peptides into a hydrophobic core and will affect the membrane binding affinity.

In the experimental fusion studies, $n_a = 4 - 5$ for the considered membrane patch size, assuming that the surface coverage is homogeneous. The significance of n_a, the number of anchors per (fixed) membrane area, is stressed by the observation that the liposome fusion rate is significantly reduced when the lipopeptide (surface) concentration is lowered [20]; an optimum was found for 0.75 mol%. A geometrical effect associated with the locking mechanism, i.e. the idea that a certain surface coverage is required for E and K peptide domains to quickly assemble into a heterodimer, is the usual explanation for this observed concentration dependence. In addition, K homomers are thought to bridge different membranes prior to mixing with complementary E decorated liposomes, for LPK concentrations up to the optimal value. The again decreased fusion rates for a higher (1 mol%) lipopeptide concentration are attributed to the formation of K homomers at the surface of the membrane prior to mixing, leading to a reduced K accessibility and a competition between homo- and heterodimer formation upon mixing [20]. We note that, since the lipid anchors are free to diffuse along the membrane, the actual value of n_a may be higher than calculated for a homogeneous surface coverage.

Using equivalent starting conditions for the lipopeptide and the same membrane composition, we extended our computational CGMD study to two ($n_a = 2$) or four lipopeptides ($n_a = 4$) of the same type

anchored in the membrane. To limit our computational effort, we restricted the latter systems to four $LP_{12}E$, containing peptide domains that have a weaker membrane affinity.

First results showed that the surface affinity of the peptide domain dominates over the lateral diffusion of the lipid anchor when the anchoring domains are initially separated by a distance. As a result, peptide domains adhere independently, in a manner that is very similar to previously discussed for the solitary case. When we insert the anchoring domains at a very short distance, however, a homo-dimer ($n_a = 2$) or homo-tetramer ($n_a = 4$) is initially formed in solution (see Figs. 8a and 9a).

While the hydrophobic residues (green and yellow) in the E/K *heterodimer* form a distinct hydrophobic core, via opposite arrangement (see SI), the situation for the homodimers E/E and K/K differs (see Fig. 8a for the representative E/E case). It is likely that the lipopeptide anchoring points and/or spacer play a role in the alignment of the hydrophobic residues at one side of the dimer, as they restrict the conformations of the peptide domains. As a result, the hydrophobic domain in the complex is insufficiently shielded from the water and the dimer disassembles, with one peptide adhering to the membrane. The lipids in close vicinity can be seen to be partially pulled out, as if to shield the hydrophobic groups of the peptide domain that is still in solution. Similar (transient) membrane destabilization has previously been observed upon insertion of cylindrical nanotubes into a lipid membrane [32]. During the next stage, also the other peptide domain adheres and finally both peptide domains diffuse independently along the membrane surface. The latter behavior is equivalent to the one for peptides that are initially anchored at a distance.

The behavior after the formation of a homo-tetramer is more intriguing, see the situation for four $LP_{12}E$ in Fig. 9. After the formation of a tetramer in solvent, only two peptide domains in the original tetramer adhere to the membrane in the usual way, with their hydrophobic residues buried deepest into the membrane. Their backbones, however, adopt a parallel orientation with respect to each other, while the other two peptide domains remain in solution. The arrangement visualized in Fig. 9b and c was found stable for 10 μs of simulation. As can be clearly seen, the hydrophobic residuals of the individual peptides in the stable homo-dimer do form a hydrophobic core in this case, by pointing in the same direction, which contributes to the stability of the homodimer. Moreover, the membrane remains flat. The observed long-term stability of the arrangement in Fig. 9b, which is in contrast with the binding and independent surface diffusion for the dimeric case in Fig. 3, suggests that all four peptide domains contribute to the stabilization of the homodimer in solution.

We conclude that, for a higher lipopeptide (surface) concentration, di- or tetra-homomers may be formed, which have a direct influence on the peptide–membrane affinity and a potential impact on fusion. In the case of tetramers, for example, not all peptide domains adhere to the membrane; the enhanced accessibility of the peptide domains that are outside the membrane, for partnering with complementary peptide domains anchored to opposing membranes, is important for the locking mechanism that precedes fusion. Since the diffusion of anchors is slow, homomer formation is sensitive to the surface coverage, where 'slow' relates to the timescale of peptide–peptide and peptide–membrane association. When only two lipopeptides are anchored closely, less stable conformations follow a two-step process of homodimer disassociation into individual peptides that bind individually and diffuse laterally along the membrane surface. This process gives rise to (transient) destabilization of the membrane. For a tetramer, two peptides were found to adhere to the membrane into a very stable arrangement with the remaining two peptide domains in solution, and we observed no significant lateral diffusion of the bound peptides.

3.3. Variation of the membrane properties

In cell membranes, the role of local membrane properties is important, as different lipids are known to form larger membrane domains that are rich of one lipid type, providing specific functionality. Increasing only the DOPE content of the DOPE:DOPC membrane was previously found to enhance PEG mediated liposome fusion [33]. Also the previous CGMD study of a short lipopeptide [13] observed binding for a 'bacterial' bilayer (a POPE:POPG mixture) but no binding for a 'mammalian' (POPC) bilayer, and concluded that electrostatics is the primary driving force for binding. The role of electrostatics is subtle, however, as ions from the solvent bind to a different lipid membrane in a different manner and change its structural and charge properties depending on the local ion concentration. Also the molecular packing density, reflected in the average area per molecule A, will have an effect on the membrane–peptide interactions, as lipids/cholesterol have to rearrange to enable peptide–membrane association. We thus focus on the membrane itself and study how particular membrane properties affect the binding of solitary lipopeptides. We introduce the terminology 'falling time' to refer to the simulation time needed for the lipopeptide to first adhere to the membrane.

The 'standard' membrane used in this study was chosen to mimic the experimental conditions [25], a DOPC:DOPE:CHOL mixture with 50:25:25 mol% composition, providing a membrane thickness of $h = 4.60 \pm 0.035$ nm and average area per molecule of approximately $A = 0.53$ nm^2. We note that the bilayer thickness has been determined from the distance between the peaks in the density of the phosphate moiety, while the area per molecule has been calculated as the area of the simulation box (in the membrane plane) divided by half the sum of the lipids and cholesterols. Taking into account the simulation temperature of 20 °C, our calculated area per molecule is in line with the

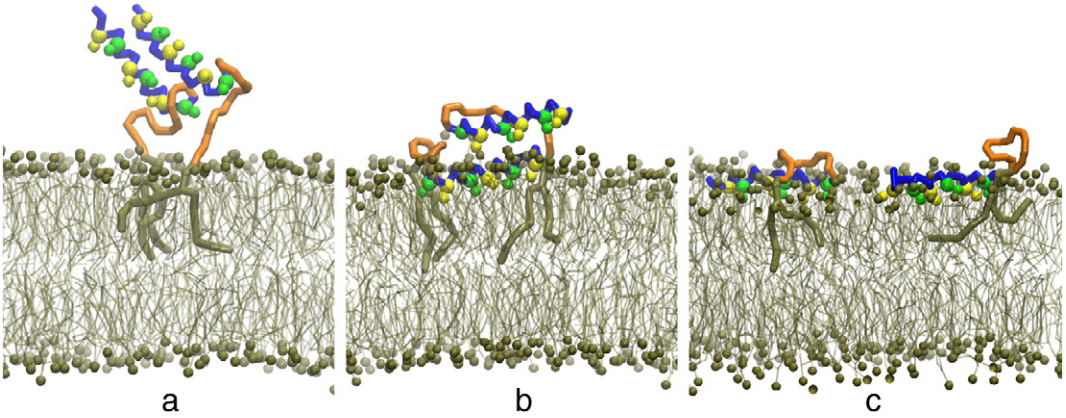

Fig. 8. Three simulation snapshots for two $LP_{12}E$ that are initially anchored at a short distance. From left to right: a) homo-dimer formation in solution; b) binding of one peptide and c) separation of the homo-dimer into individual lipopeptides that diffuse along the membrane surface. The color code is identical to the one in Fig. 3.

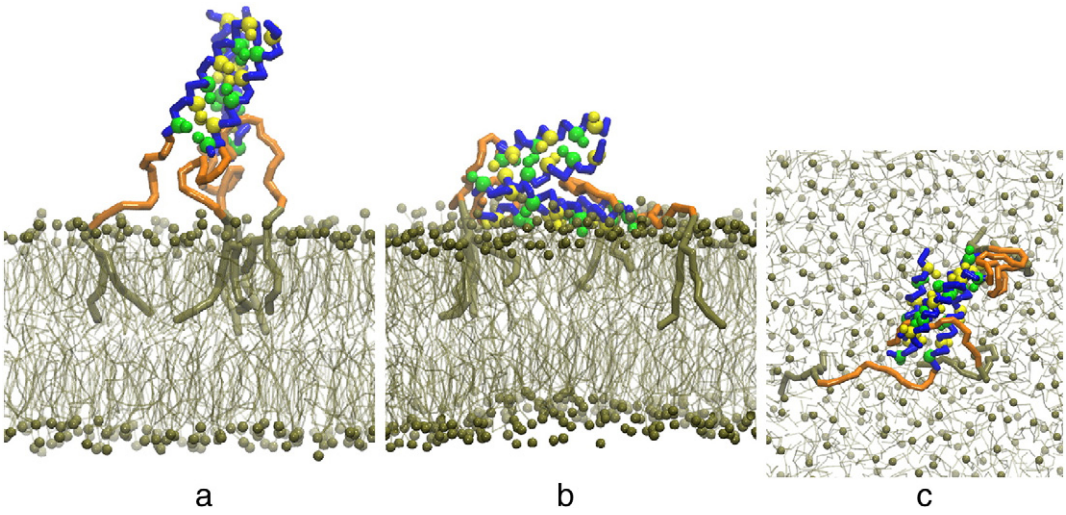

Fig. 9. Two simulation snapshots for four $LP_{12}E$. From left to right: a) tetramer formation in solution; b) stable conformation after long (20 μs) simulation, with two lipopeptides of the original tetramer attached to the membrane surface and one homo-dimer in solution; c) top view of b). The color code is identical to the one in Fig. 3.

few values available in the literature for related membranes: 0.76 nm^2 for pure DOPC, 0.72 nm^2 for pure DOPE, 0.65 nm^2 for DOPC:CHOL (80:20) and 0.62 nm^2 for DOPE:CHOL (80:20) at 25 °C [35], and 0.58 nm^2 for DOPC:CHOL (75:25) at 30 °C [36]. Note also that the presence of sodium chloride is known to slightly decrease the area per lipid.

Despite our efforts to closely reproduce the experimental membrane, one should realize that the mapping between the atomistic and coarse-grained lipids is limited in terms of resolution, meaning that a hydrocarbon chain of $n = 18$ or 20 at the atomistic level is represented by the same lipid at the coarser MARTINI level. Detailed analysis of X-ray and neutron scattering data has shown that the tail length and the position of the double bond have a small but notable effect on the area per lipid A [26]. To consider the effect of this model limitation, we have performed simulations of five additional membranes (listed in Table 2) in the same lipopeptide setting (see membrane preparation in the Methods section). In this way, we extend the membrane properties and study the effect of large membrane domains, that may form, on lipopeptide binding.

The membrane always contains one DOPE anchor of the lipopeptide (the previous standard membrane is type I). All membranes were prepared and equilibrated for 0.4 μs with position constraints on the peptide domain of the lipopeptide in the solvent. Structural properties of the equilibrated membrane can be found in Table 2. To avoid any complications due to the exact cholesterol localization (in or outside the leaflet), here we give only the total area of the simulation box A^{tot} and not the area per molecule. After equilibration, the constraint on the peptide is released and this part of the trajectory is used for analysis (Table 2).

Concentrating on the role of the membrane surface energetics on the peptide behavior, we see that reversing the lipid composition, i.e. more DOPE than DOPC (type II vs type I), leads to a closer lipid packing: a small increase of the thickness of the hydrophobic membrane domain and decrease in the total area. This is expected since the head group repulsion is smaller for NH_3(PE) compared with NC_3(PC). No major effect is observed on the falling time for both peptide domains, which remains roughly equal to the average time determined for membrane type I.

By removing all cholesterol molecules (type III), we probe the effect of de-condensation [10,37]: the total area is smaller while the cross-sectional area per molecule (lipid only, in this case) increases to $A = 0.63$ nm^2. The lipids are more disordered and the membrane thickness is smaller. The behavior of peptides attached to the type III membrane is very similar to the behavior for type I.

More evident membrane modifications are obtained after either variation of the hydrocarbon tail length or by replacing some or all lipids by alternatives that allow for closer packing. Here, we consider the second option and replace DOPE and/or DOPC lipids by fully saturated DSPC lipids (the head group charge is not affected). As seen from the significantly reduced area and increased thickness in Table 2, increasing the DSPC content indeed leads to a closer lipid packing. Replacing DOPC by DSPC, membrane type IV, leaves the K behavior almost unaffected, while it takes the E peptide domain roughly 1.5 μs to approach the membrane surface and associate. The incorporation of the E domain in the membrane is, however, only partial within simulation time (10 μs) and at a much shallower location with respect to the membrane surface than for the standard membrane (type I). In the type V membrane, where also the DOPE is replaced by DSPC, the time observed for the K domain to associate with the membrane increases to 2.5 μs, while the E domain remains in the solvent phase during the full 10 μs trajectory. Finally, for a pure DSPC membrane (type VI), the area per lipid reduces to 0.47 nm^2, meaning that all lipids are closely packed. As a consequence, the membrane is not in the fluid phase anymore, but it experiences a phase transition to a gel during membrane preparation. The lipid diffusion rates along the membrane are considerably reduced compared to the other systems. From independent simulations for each peptide, we find that both E and K domains in the lipopeptide remain in the solvent phase during 10 μs of simulation. Since the membrane surface energetics is only marginally affected by the replacement of DOPE/DOPC by DSPC, clearly the lipid rearrangement that is required to make space for the peptide is the most important limiting factor.

We can use these simulations to recognize trends. The first trend is that the time for individual peptide domains to associate with the membrane increases with a decreasing lipid per area. Second, the K peptide apparently experiences a higher membrane affinity than the E peptide, in agreement with our earlier conclusion. Our last finding, i.e. that both peptide domains do not bind within simulation time for the densest

Table 2
The composition, total membrane area A^{tot} and membrane thickness h of the considered membranes, simulated at T = 293 K. The membrane considered in all other sections is type I. One DOPE lipid, the anchor for the lipopeptide, is always part of the membrane.

Type	Composition				Structural properties		Adhered	
	DOPC	DOPE	CHOL	DSPC	A^{tot}(nm^2)	h(nm)	E	K
I	192	96	96	–	101.64 ± 0.29	4.60 ± 0.035	Yes	Yes
II	96	192	96	–	100.16 ± 0.49	4.64 ± 0.068	Yes	Yes
III	192	96	–	–	91.35 ± 0.57	4.56 ± 0.11	Yes	Yes
IV	–	96	96	192	88.05 ± 1.51	5.15 ± 0.080	Partial	Yes
V	–	1	96	287	82.25 ± 0.05	5.40 ± 0.060	No	Yes
VI	–	1	–	287	67.70 ± 0.09	5.62 ± 0.043	No	No

membrane, agrees very well with the experimentally measured peptide unbinding from a monolayer when the monolayer is slowly compressed beyond a certain 'critical' area [30]. These experiments determined a smaller critical value for LPK than for LPE, meaning that E peptide domains unbind for less dense monolayers, and we conclude that there is very good qualitative overall agreement between the simulated and experimental results. A quantitative comparison is complicated by the experimental setup, e.g. individual bound peptides are beyond the experimental resolution, and the induced α-helical peptide structure that was used in these simulations, which will shift these critical values. Nevertheless, the computational finding that peptides do not bind, despite an increased driving force for binding due to the imposed secondary peptide structure, corroborates a decreased propensity for association of solitary lipopeptides with denser membranes.

3.4. Sensitivity of membrane binding to the peptide secondary structure

An α-helical secondary structure was determined for both E and K peptides in the hetero-dimeric state and/or in association with a lipid membrane [30], albeit that the peculiarities slightly differ due to the strain that individual α-helices experience when assembled in a coiled-coil. However, short MD simulations suffice to show that an α-helical secondary structure unwinds for solitary E or K peptides in solution (see SI). Since the interactions that regulate secondary structure formation (hydrogen bonding) are generally not represented after the coarsening procedure, this adaptivity to the local environment is absent in the standard coarse-grained model for the peptides.

In the usual MARTINI approach, a helical secondary structure is imposed by standard torsion potentials between each four consecutive backbone particles, with an equilibrium angle of $\phi = 60^\circ$ and a large force constant of 400 kJ mol^{-1}. This treatment, which effectively dictates 100 % peptide helicity during simulation, has been used in all previous sections. Here, we decrease the force constant for the torsion potentials from 400 to 4 kJ mol^{-1}. All other parameters, including those for the membrane, and the membrane preparation are 'standard'. Although this change may be considered too drastic, secondary structure restraints were completely lifted for a much shorter lipopeptide system [13]. Our chosen value is high enough to acknowledge the peptide propensity for α-helix formation within the membrane, against thermal fluctuations, but small enough to enable a (mild) secondary structure modulation. In the remainder, we refer to the original setup as helix and the new setup as coil.

With the α-helix no longer stringently imposed, the peptides adapt their conformation quickly to shield hydrophobic groups from the surrounding solvent (by bending), first transforming into a globular structure (see Fig. 10a). The globular, hairpin-like secondary structure, which shields the hydrophobic residuals from the surrounding solvent, clearly shows the propensity for an α-helical motive in part of the peptide.

After this stage, the coil peptides approach the membrane as before and adhere to it. Once in the membrane, the peptides undergo a process of folding: they straighten up and the helix is reconstituted. Evidence of this membrane-induced secondary structure formation can be found in the snapshot in Fig. 10c. Additional insight can be obtained from the peptide end-to-end distance distribution in the initial stages (peptide outside the membrane) and at the end of simulation (last microsecond of a 6 microsecond simulation trajectory with the peptide inside the membrane) shown in Fig. 11. The reference end-to-end distance, taken from the standard forced α-helical coarse-grained representation, is 3.3 nm.

From the end-to-end distributions, we see that the initial globular conformation (small end-to-end distances) transforms into a stretched conformation, with an end-to-end distance that peaks around the reference value for an α-helical secondary structure (3.3 nm). This peak is more prominent for the K than for E peptide domain, which has a rather broad distribution. From the calculated density profiles (see Fig. S4), we find that the Ile and Leu amino acids are again most deeply submerged into the membrane for both peptides, but also that the E peptide domain as a whole penetrates deeper into the membrane in comparison to its helix-imposed counterpart (see Fig. 6), giving rise to overlapping E and K density profiles for the coil case. Visual inspection provides additional information, and shows that both peptide domains adapt to the presence of the membrane by positioning their hydrophobic residuals downwards, while their overall globular shape initially does not change, see Fig. 10a and b for the K peptide. While the K peptide domain shows a clear tendency to straighten up, see Fig. 11, the increased penetration depth for the E peptide domain points at partial screening of negatively charged residuals when the E peptide is the hairpin conformation. As a result, the driving force for straightening up is reduced and a broad end-to-end distribution is observed for the E peptide, see Fig. 11.

To further quantify the stretched conformation of the K peptide domain in terms of helicity, we plot the simulated angular distribution for all 16 torsion angles ϕ_i. For clarity, Fig. 12 shows only the most specific angular distributions before and after peptide binding to the membrane; we number angles starting from the free side of the peptide. We find that the distributions for $i \in \{4, 7, 11, 14\}$ evolve from a rather broad distribution to a peaked distribution around $\phi \in [50^\circ, 60^\circ]$ (see black, red, blue and cyan in Fig. 12). The distributions for three angles, $i \in \{9, 10, 16\}$, initially peak in the same range (see green for a representative example) but evolve into a somewhat skewed distribution around a larger angle $\phi \in [80^\circ, 90^\circ]$. For the remaining angles, the distributions initially also peak in the $\phi \in [50^\circ, 60^\circ]$ range, but they are not significantly affected by binding of the peptide to the membrane (illustrated by gray). As a reference, we have also plotted the equilibrium angle distribution for the considered torsion potential ($k_\phi = 1.6 k_B T$ at room temparature) in Fig. 12b (dotted line).

The results show that the simulated angular distributions for most angles are much narrower than imposed by the torsion potential, which, in combination with visual inspection, signals enhanced internal structuring even when the peptide domain is in solution. When bound to the membrane surface, the K peptide straightens up as a whole to form an α-helix, as suggested by the end-to-end distance peak around 3.3 nm, but close inspection of the angular distributions shows that the α-helical structure is slightly distorted. Since the membrane acts as a template for this process, inducing the secondary structure transition by the surrounding lipids and cholesterol molecules, this distortion can be explained in terms of a template mismatch.

Concluding, we find that peptide binding to the membrane does not crucially depend on the secondary structure of the peptide domain. During the simulations, both E and K lipopeptides (in the coil conformation) adhere to the membrane, and the peptide domains adapt an extended conformation, which is enhanced in K compared to E, with the hydrophobic residues buried deep into the bilayer, similar to the peptide with imposed α-helix. Moreover, as the interactions that govern helix formation are only weakly inferred in this setup, it highlights the role of membrane-templating in the experimental finding that the peptide domain is in a helical conformation when bound to the membrane [30].

4. Discussion

Characterizing the concerted molecular action in the liposome fusion process is of major importance for the understanding and control of many important biological processes in which cells, intracellular compartments or viral particles make contact. Based on this information and the validated computational methodology, novel peptides with improved functionality for fusion may be designed, with vital applications in drug delivery.

Since the experimental insight into processes that take place at the molecular level is limited, the molecular fusion scenario remains a matter of speculation. One suggestion in the literature is that bound peptides can mediate fusion if the liposomes come in contact by chance and conjugated peptides interact with each other to disturb the membrane [42]. Our computational study concentrated on a more likely

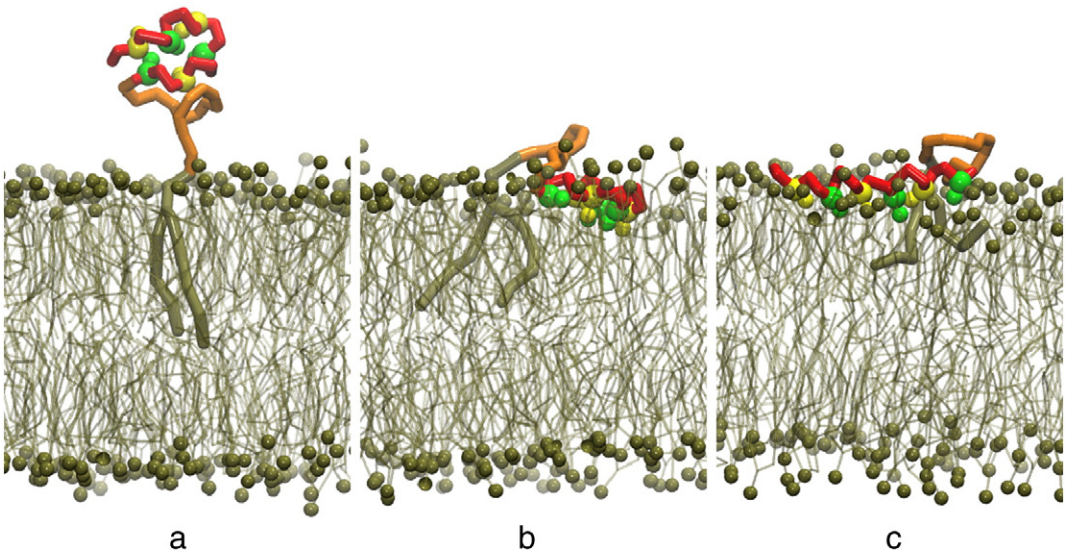

Fig. 10. Three representative snapshots for a $LP_{12}K$ lipopeptide (coil) interacting with the membrane: (a) prior to falling, (b) immediately after falling and (c) after 6 μs at the membrane surface. The color code is identical to Fig. 3a.

scenario and focused on the question under what conditions fusogenic lipopeptides LPK and/or LPE reside in the solvent phase. Good peptide accessibility is important, since the locking step crucially depends on the formation of hetero-complexes between opposing membranes. However, the computationally predicted preference of both individual peptides to locate their hydrophobic face partially inside the membrane suggests a significantly reduced probability for E/K hetero-dimer formation. Moreover, the observed membrane deformations upon individual peptide attachment are insufficient to induce membrane remodeling. Varying the lipopeptide surface concentration, we found that LPE is accessible in the solvent phase as a homodimer, which is stabilized by two of the same peptides on the membrane surface. This introduces the possibility of E peptide binding to an opposing membrane and consequent formation of a bridging hetero-dimer with a complementary (bound) K peptide. Our results therefore suggest that the lipopeptide surface concentration, which was experimentally identified as key to fusion, plays a much more intriguing role than previously assumed. It is particularly vital for the locking mechanism, as the local lipopeptide concentration regulates the (dynamic) balance between membrane-bound peptides and membrane-unbound peptide aggregates. We therefore conclude that the usual peptide pair design criteria towards the prevention of homomer formation (by electrostatic interactions) have a devastating effect on fusion if fulfilled. One may speculate, based on the simulations for two anchored lipopeptides, that binding–unbinding phenomena play a role in membrane distortion.

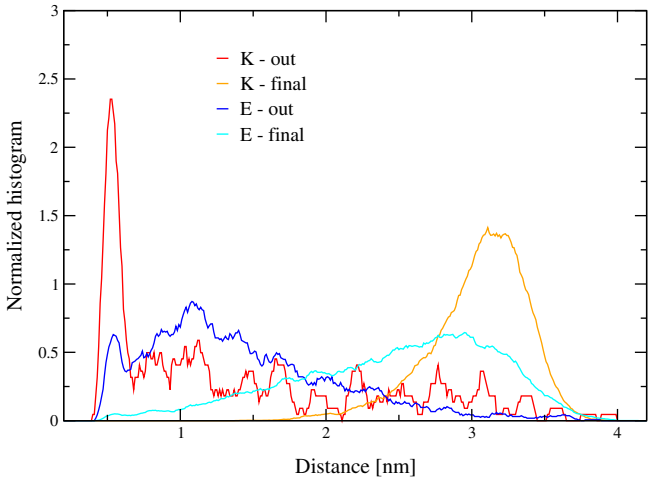

Fig. 11. The normalized distributions of the end-to-end distance in K and E coil peptides for the simulation times in which the peptides are well outside the membrane (red and blue curves) and at the end of equilibration, at the top of the membrane (orange and cyan).

Apart from using validated force fields, our simulation results were found to compare favorably with the few detailed experimental findings that are available for this system [30], both in terms of the membrane affinity (K stronger than E) and membrane-bound peptide domain orientation, and in the trends for peptide unbinding upon membrane compression, which we mimicked by reducing the average area per lipid. The length of the polymer spacer was also varied experimentally, but the only notable effect on the fusion rate was identified for very short spacers, and results were never published. We review our findings for two additional spacer lengths in the Conclusion section, but refer to the Supporting Information for details of the computational results.

In terms of future efforts, we hope that these first molecular guidelines will stimulate experimental research on this and related model fusion system and inspire a more targeted experimental investigation of molecular mechanisms that play a role in fusion. On the computational side, there are two clear options to go beyond the current study: (1) coarse-grained molecular conformations may be imported into an all atom model (see the SI) and used for further validation and study of mechanisms beyond the coarse-grained resolution, like snorkeling, and (2) the current coarse-grained model can be applied to study molecular mechanisms in actual fusion events. Nevertheless, there are computational restrictions associated with both options. The time/length scales that are tractable by atomistic simulation are short/small, respectively, rendering simulation of much smaller subsystems a necessity. Simulating fusion events by coarse-grained methodology is not straightforward. Selecting two decorated flat membrane patches in close vicinity is problematic due to the boundary conditions, which introduce a bias in terms of an artificial stress on the membrane, while simulating two decorated liposomes of a realistic 50 nm diameter is at the border or beyond the current computational capacity. An additional coarsening step for at least one of the constituents may be desired and the recently hybrid MD-SCF method is a good candidate [32]. Also the electrostatic interactions in the current setup may be reconsidered. The recently developed polarizable MARTINI water model [40] is frequently proposed for resolving the ion-binding discrepancy of the standard water model, which we treated by increasing the salt concentration, but it comes with a severe

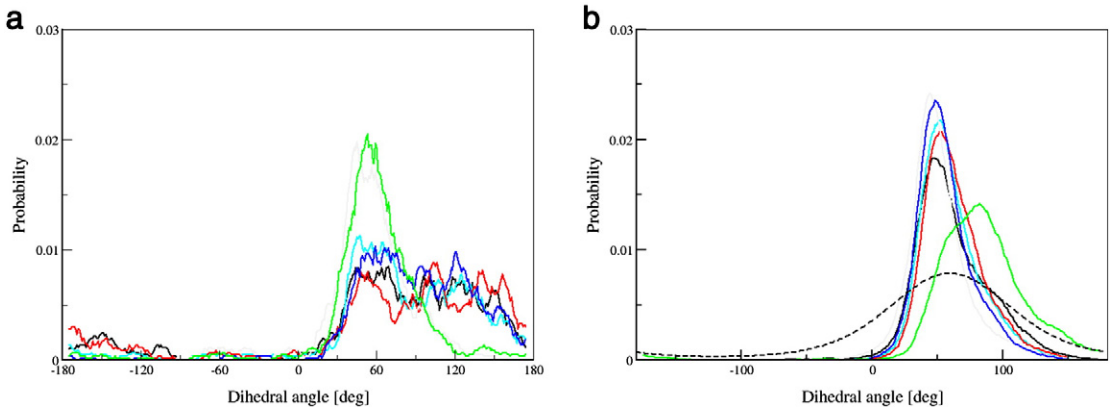

Fig. 12. Histograms of selected dihedral angles along a peptide K at (a) the beginning of the simulation, when the peptide K is outside the membrane, in a hairpin shape and (b) the last microsecond of a 7 microsecond trajectory when the peptide is at the membrane surface, in an elongated shape. Colors identify the same torsion angles in (a) and (b). Only exemplary cases are shown for distributions that follow the same trends (green: shift of peak position and skewing, and gray: no significant change). As a reference, the normalized equilibrium distribution $exp(-\Phi/k_BT)$, with Φ the torsion potential, is shown as a dotted line in (b).

computational penalty. Our results, and previous validation studies performed using the standard MARTINI model, give us some confidence that our current treatment is sufficient, and that simulation using this new polarized model will not seriously change the main outcomes of this study.

5. Conclusions

We carried out extensive coarse-grained molecular dynamics simulations to characterize the membrane binding affinity of lipo-peptides LPE and LPK (E and K peptides linked to a DOPE lipid from the membrane via a polymer linker). In order to cover the diversity of experimental conditions, we studied the influence of (1) the secondary structure of the peptide components, (2) the membrane structural properties, and (3) the length and composition of the linker between lipid and peptide. Our results indicate that peptide domains in solitary lipopeptides adhere to the membrane surface, adopting a parallel orientation with the bilayer, with the hydrophobic amino-acids inserted into the lipid head-group region, in full agreement with the experimental findings. This binding behavior does not depend on the secondary structure of the peptide domain. Both E and K lipopeptides in helix-relieved conditions adhere to the membrane and adopt very similar conformations compared with their helix-imposed counterparts. Moreover, a reverse transition of the peptides to a helical secondary structure is observed after binding, highlighting the role of the membrane as a template (partitioning–folding coupling). Two general exceptions were found for which the peptide domains remain in the solvent phase: for membranes with very small area per lipid and for supra-molecular homo-aggregates of the peptides. From the latter case, we concluded that the lipopeptide concentration plays a vital role in regulating the dynamic balance between membrane-bound peptides and membrane-unbound peptide aggregates. The length of the polymer spacer is irrelevant for the LPK lipopeptide, while for LPE a better accessibility in the solvent phase has been observed for intermediate length (4 PEG units compared with 0 or 12 units). More visible effects were observed when the succinic anhydride is included or excluded as a linker. As determined experimentally [30], the membrane affinity of the E peptide is weaker than for the K peptide.

Our findings indicate that peptide–peptide interactions are important in membrane fusion and suggest a new fusion scenario with a prominent role of homomers. As destabilization of homomers is usually an important design criterion, the current study offers valuable information for analyzing and further improving the fusion models in the laboratory, with possible benefits for improved applications in drug delivery.

To provide additional understanding of the membrane fusion mediated by LPE and LPK lipo-peptides, a subsequent study of the assembly of E and K peptides is in preparation.

Acknowledgements

This research was financed by the BioSolar Cells open innovation consortium, supported by the Dutch Ministry of Economic Affairs, Agriculture and Innovation. We are grateful for the computing time allocated by The Netherlands Computing Facilities (NCF) to perform part of the calculations presented in this paper. We thank our colleagues from the Supramolecular & Biomaterials Chemistry Group at Leiden University – Martin Rabe, Harshal Zope and Giuliana Martelli – for useful discussions.

Appendix A. Supplementary data

Supplementary data to this article can be found online at http://dx.doi.org/10.1016/j.bbamem.2014.12.010.

References

[1] L.V. Chernomordik, M.M. Kozlov, Membrane fusion, Current Topics in Membranes 68, Elsevier, New York, NY, 2011.
[2] H. Robson Marsden, I. Tomatsu, A. Kros, Chem. Soc. Rev. 40 (2011) 1572.
[3] H. Robson Marsden, N.A. Elbers, P.H.H. Bomans, N.A.J.M. Sommerdijk, A. Kros, Angew. Chem. Int. Ed. 48 (2009) 2330.
[4] S.S. Pendley, Y.B. Yu, T.E. Cheatham III, Proteins — structure functions and, bioinformatics, 74 (2009) 612.
[5] S.J. Marrink, H.J. Risselada, S. Yefimov, D.P. Tieleman, A.H. de Vries, J. Phys. Chem. B 111 (2007) 7812.
[6] L. Monticelli, S.K. Kandasamy, X. Periole, R.G. Larson, D.P. Tieleman, S.J. Marrink, J. Chem. Comput. 4 (2008) 819.
[7] H. Lee, A.H. de Vries, S.J. Marrink, R.W. Pastor, J. Phys. Chem. B 113 (2009) 13186.
[8] J.N. Horn, J.D. Sengillo, D. Lin, T.D. Romo, A. Grossfield, Biochim. Biophys. Acta 1818 (2012) 212.
[9] X. Periole, A.M. Knepp, T.P. Sakmar, S.J. Marrink, T. Huber, J. Am. Chem. Soc. 134 (2012) 10959.
[10] A. Rzepiela, D. Sengupta, N. Goga, S.J. Marrink, Faraday Discuss. 144 (2010) 431.
[11] L. Janosi, Z. Li, J.F. Hancock, A.A. Gorfe, PNAS 109 (2012) 8097.
[12] Z. Li, L. Janosi, A.A. Gorfe, J. Am. Chem. Soc. 134 (2012) 17278.
[13] H. Robson Marsden, A.V. Korobko, T. Zheng, J. Voskuhl, A. Kros, Bionmat. Sci. 1 (2013) 1046.
[14] B. Hess, C. Kutzner, D. van der Spoel, E. Lindahl, J. Chem. Theory Comput. 4 (2008) 435.
[15] M. Bulacu, X. Periole, S. Marrink, J. Biomacromole. 13 (2012) 196.
[16] G. Rossi, L. Monticelli, S.R. Puisto, I. Vattulainen, T. Ala-Nissila, Soft Matter 7 (2011) 698.
[17] H. Robson Marsden, Extending the Self-assembly of Coiled-coil Hybrids(Thesis) 2009.
[18] N. Kucerka, J. Gallova, D. Uhrikova, P. Balgavy, M. Bulacu, S.J. Marrink, J. Katsaras, Biophys. J. 97 (2009) 1926.
[19] J.R. Litowski, R.S. Hodges, J. Biol. Chem. 277 (2002) 37272.
[20] L.D. Schuler, W.F. van Gunsteren, Mol. Simul. 25 (2000) 30119.
[21] P. Lague, B. Roux, R.W. Pastor, J. Mol. Biol. 354 (2005) 1120.
[22] M. Rabe, C. Schwieger, H.R. Zope, F. Versluis, A. Kros, Langmuir 30 (2014) 7724.
[23] T. Apajalahti, P. Niemelä, P. Govindan, M.S. Mietinen, E. Salonen, S.J. Marrink, I. Vattulainen, Faraday Discuss. 144 (2010) 411.

[24] E. Sarukhanyan, A.D. Nicola, D. Roccatano, T. Kawakatsu, G. Milano, Chem. Phys. Lett. 595 (2014) 156.
[25] M.E. Haque, T.J. McIntosh, B.R. Lentz, Biochemistry 40 (2001) 4340.
[26] R.S. Cantor, Biophys. J. 76 (1999) 2625.
[27] W.C. Hung, M.T. Lee, F.Y. Chen, H.W. Huang, Biophys. J. 92 (2007) 3960.
[28] T.P.W. McMullen, R.N.A.H. Lewis, McElhaneyR.N. , Curr. Opin. Colloid Interface Sci. 8 (2004) 459.
[29] J.P. Segrest, M.K. Jones, V.K. Mishra, G.M. Anantharamaiah, Current Topics in Membranes, 52, 2002, p. 397.
[30] J.P. Segrest, H. De Loof, J.G. Dohlman, C.G. Brouillette, G.M. Anantharamaiah, Proteins Struct. Funct. Genet. 8 (1990) 103.
[31] S.O. Yesylevskyy, L.V. Schafer, D. Sengupta, S.J. Marrink, PLoS Comput. Biol. 6 (2010) e1000810.
[32] S. Baoukina, D.P. Tieleman, Biophys. J. 99 (2010) 2134.